Measurement-Induced Relative-Position Localization Through Entanglement

A. V. Rau,* J. A. Dunningham, K. Burnett

We consider the localization of a pair of particles in relative-position space. We show how a sequence of scattering interactions progressively entangles two particles, giving rise to a robust state of well-defined separation and thus providing a natural description of relative position. We use two thought experiments to describe the localization process. The first is an interferometer with recoiling mirrors. The second, and more general, case considers photons scattering from a pair of particles and the resulting emergence of a Young's interference pattern. The underlying framework of the localization process suggests a prominent role for entanglement and relative observables at the boundary between quantum and classical mechanics.

One question central to an understanding of the boundaries between quantum and classical physics is how objects localize in position space. The rules of quantum mechanics permit superposition states, allowing objects to be spread across space. The classical world, on the other hand, is composed entirely of objects with well-defined positions. One of the most successful descriptions of this transition between the microscopic and macroscopic is the theory of decoherence, in which a system is coupled to an environment with many degrees of freedom, causing the decay of its macroscopic coherences (*1*–*5*). In practice, however, decoherence theory is often difficult to apply, because of the complex nature of the environment and its influence on the system. We present here a simpler approach, from the perspective that all measurements of position are intrinsically relative measurements, that eliminates the need for environmental dissipation by focusing instead on entanglement between objects. We show how a sequence of such measurements entangles two particles, naturally leading to robust semiclassical states of well-defined relative position.

Our model for the localization process involves a sequence of external scattering interactions with a system of two arbitrary, noninteracting particles of equal mass. During each event, a photon or some other particle with definite momentum scatters off the system and is detected. The description of the interaction relies only on momentum conservation: The change in the photon's momentum, Δk, results in an equivalent momentum kick to the two-particle system. Because only the scattered photon is observed, the detection event (a click) yields no information about which of the two particles it interacted with. The result is therefore a superposition of the effects of the photon scattering off one particle with that of it scattering off the other. It is this lack of information and subsequent projection of the quantum state, similar to that established in the case of a single spontaneous emission from a pair of excited atoms (*6*), that entangles the two particles and drives the localization process.

To illustrate the general effect, consider two particles in a momentum product state, with undefined initial relative and absolute positions. The result of a scattering event, after the detection of the photon, is a linear combination of the results of the photon hitting each particle (*7*)

$$|p_1\rangle|p_2\rangle \longrightarrow c_1|p_1 + \Delta k\rangle|p_2\rangle + c_2|p_1\rangle|p_2 + \Delta k\rangle \quad (1)$$

where $p = \hbar k$, $\hbar$ (Planck's constant h divided by 2π) is set at 1, and the c_i values are probability amplitudes. The two particles are now in an entangled state, with a definite center-of-mass (cm) momentum, $|p_1 + p_2 + \Delta k\rangle_{cm}$. The center of mass remains in a shifted momentum eigenstate throughout the entire localization process, meaning that neither particle ever has a well-defined absolute position. We therefore ignore the center-of-mass component and work only in the relative coordinate. Assuming that both particles scatter light identically, each term in the superposition should have an equal weighting, $|c_1| = |c_2|$. After removing the common phase, the general scattering relation in relative (rel) coordinates then reduces to

$$|p_0\rangle_{rel} \longrightarrow \frac{1}{\sqrt{2}}\left[|p_0 + \frac{\Delta k}{2}\rangle_{rel} + e^{i\phi}|p_0 - \frac{\Delta k}{2}\rangle_{rel}\right] \quad (2)$$

where [$p_0 \equiv (p_1 - p_2)/2$].

The relative phase, ϕ, between the two possible events is related to any observed interference between the alternative paths of the photon at the detector and will turn out to be critical to the emerging relative position of the two particles. We will return to the interference pattern of the scattered photons later. Eq. 2 demonstrates that the scattering process has broadened the relative-momentum wave function; the conjugate effect is reduced uncertainty in relative-position space. This is the basis of the localization process, because the particles become increasingly entangled and their relative position better defined with each scattering event [for a discussion on quantifying entanglement, see (*8*)].

One might think that we could localize a single particle to a definite position by a similar but more conventional procedure. However, observing a photon scattered off a lone particle yields no position information: The particle simply recoils, shifting its momentum wave function without any effect on its spatial distribution. Only when there is an extra element in the interaction, such as a lens in the case of Heisenberg's microscope, can we gain any position information and thus localize the particle, as has been demonstrated by Holland *et al.* (*9*). It is then entangled with the lens, and its position is determined relative to the axis of the lens, which is consistent with our earlier description of the localization process (*10*).

Before discussing the general case of scattering from free particles, it is helpful first to analyze the localization process for two mirrors arranged in a type of Mach-Zehnder interferometer (Fig. 1). The mirrors, the target particles in this thought experiment, can recoil, but are constrained to move along one dimension. A photon of known momentum, k_γ, is incident upon a beam splitter and sent down two alternative paths, a and b, along each of which it hits a mirror. Assuming specular reflection, the momentum transferred to each mirror can be given by $\Delta k = 2k_\gamma \cos(\alpha)$, where α is the angle of incidence. The paths are recombined by a second beam splitter, whose two output ports are under observation by detectors. Because each scattering event involves a single photon, only one detector at a time will record a click.

We take the wave function of the mirrors before a scattering event to be a general superposition, $|\psi_n\rangle = \Sigma_r\, c_r\, |r\rangle$, where $|r\rangle$ is a state of definite relative position r with amplitude c_r. From Fig. 1, it is clear that $r > 0$, as the arms of the interferometer cannot overlap and must each be identified with a particular mirror. The photon state after the first beam splitter, M, is given in terms of the

Clarendon Laboratory, Department of Physics, University of Oxford, Parks Road, Oxford OX1 3PU, UK.

*To whom correspondence should be addressed. E-mail: a.rau@physics.ox.ac.uk

occupation numbers, $|n_a,n_b\rangle$, of the modes of the two arms: $|\psi_\gamma\rangle = [i|1,0\rangle + |0,1\rangle]/\sqrt{2}$. From its conjugate nature, $\hat{r}$ is the generator of translations in momentum space, so the momentum kicks are represented by $\exp(i\kappa\hat{r})$, where $\kappa \equiv \Delta k/2$ is the magnitude of the kick in relative coordinates (*11*). The total state of the system just before the second beam splitter, *N*, is then

$$|\Psi_n\rangle = \frac{1}{\sqrt{2}}\sum_r c_r|r\rangle\,[ie^{i\kappa r}|1,0\rangle - e^{-i\kappa r}|0,1\rangle] \quad (3)$$

This wave function is properly normalized, because $\langle\Psi_n|\Psi_n\rangle = \Sigma_r|c_r|^2 = 1$.

Next, we consider the detection process, and the likelihood of observing the photon at a particular port. If the annihilation operator for the photon mode at detector D_1 is given by $(\hat{b} + i\hat{a})/\sqrt{2}$, the expectation value of the corresponding number operator gives the probability of detection

$$P_1 = \frac{1}{2}\langle\Psi_n|(\hat{b} + i\hat{a})^\dagger(\hat{b} + i\hat{a})|\Psi_n\rangle$$

$$= \sum_r |c_r|^2\cos^2(\kappa r) \quad (4)$$

Similarly, for D_2

$$P_2 = \frac{1}{2}\langle\Psi_n|(\hat{a} + i\hat{b})^\dagger(\hat{a} + i\hat{b})|\Psi_n\rangle$$

$$= \sum_r |c_r|^2\sin^2(\kappa r) \quad (5)$$

and $P_1 + P_2 = 1$, as required. We simulate a detection at a particular port by choosing a random outcome from this probability distribution.

The procedure for updating the mirrors' wave function after a detection is straightforward, as the projection operator is the mode operator of the corresponding port. For a detection at D_1

$$|\psi_{n+1}\rangle = \frac{1}{\sqrt{2}}(\hat{b} + i\hat{a})|\Psi_n\rangle$$

$$= -\sum_r c_r\cos(\kappa r)|r\rangle \quad (6)$$

and for D_2

$$|\psi_{n+1}\rangle = \frac{1}{\sqrt{2}}(\hat{a} + i\hat{b})|\Psi_n\rangle$$

$$= -\sum_r c_r\sin(\kappa r)|r\rangle \quad (7)$$

After renormalizing, we have the wave function of the mirrors after a single scattering event. We can then iterate the entire procedure by feeding the wave function back as the initial state of the next scattering event.

The squared magnitudes of the sinusoidal factors in Eqs. 6 and 7 act as envelopes, incorporating the effects of the scattering interaction into the relative-position probability distribution, $|\psi_n(r)|^2$, of the mirrors. Each gives the probability that an equivalent pair of classical mirrors, localized to a separation of *r*, would have produced a detection at the corresponding port. The most probable separations are where the envelope peaks; repeated detections of photons with the same momentum at this port would drive the relative position of the mirrors toward these values. Its zeros indicate separations that cannot result in a detection at that port and so must be ruled out.

Fig. 2 shows a sequence of snapshots of $|\psi_n(r)|^2$ for one particular simulation of the localization process. A monochromatic photon source is tuned to give identical momentum kicks of $\kappa_0 = k_\gamma\cos(\alpha)/2$ each scattering interaction. The mirrors are initially in a state of ill-defined relative position within a region of finite size *L*, many times the wavelength of the light: $|\psi_0(r)|^2$ is a constant for $L \geq r > 0$, and zero elsewhere. Given Eqs. 4 and 5, the first photon is thus equally likely to be detected at either port. In this simulation, it is observed at D_2, projecting the wave function according to Eq. 7. The mirrors have begun to localize about $r = \pi/2\kappa_0$, although there is still substantial uncertainty in relative-position space, as each scattering event increases the spread in the relative-momentum distribution by only Δk (see Eq. 2). For the next scattering event, $P_2 > P_1$, because the emerging relative position of the mirrors increases the likelihood of a detection at the same port. Subsequent detections in this run do in fact occur at D_2, strengthening this feedback process and further narrowing the peak of the wave function in *r*-space. After $n = 100$ events, the mirrors have a well-defined relative position of $r = \pi/2\kappa_0$. Scattered photons are now nearly certain to be detected at D_2, as we would expect from the analogous classical interferometer.

Strictly speaking, the wave functions shown in Fig. 2 are periodic in π/κ_0 throughout *L*, as required by Eqs. 6 and 7 when the photons all have the same frequency. However, by using photons of different color, as suggested by the method of exact fractions in interferometry (*12*), we can localize the mirrors to a definite separation, which corresponds to a single peak in *L*. The procedure is the same as for the monochromatic case, except that at each iteration, the magnitude of the momentum kick is chosen from some distribution, $P(\kappa)$. Fig. 3 shows a representative outcome for $L = 4\pi/\kappa_0$, set against the periodic $n = 100$ wave function of the monochromatic case in Fig. 2. The new peak is much more sharply defined, even after only half as many scattering events.

Having established the framework for the process of localization, we now consider the more general case of light scattering off a pair of particles. The scattered photons are observed on a screen in the background (Fig. 4). For simplicity, the analysis is one-dimensional—the particles move along the *x* axis in a region of finite size *L*—although it can be readily extended to higher dimensions. A photon scattered at an angle θ imparts a momentum kick of $\kappa = \Delta k/2 = k_\gamma\sin(\theta)/2$ to each particle, where the screen is in the far field. We now label the corresponding one-photon mode to the point of detection as $|\theta\rangle$ and must account for a path-length difference of $r\sin\theta$ between the photon scattering off one particle or the other. In addition, there is now a possibility of the photon passing

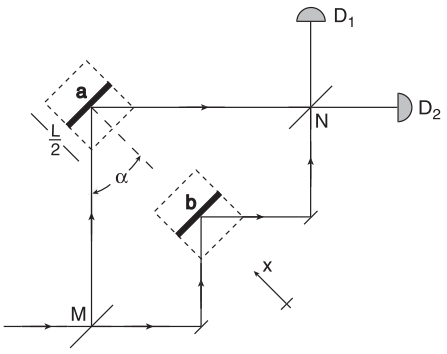

Fig. 1. The interferometer setup. A photon incident on beam splitter *M* is sent down two alternative paths, to interact with mirrors *a* and *b*, which are aligned normal to the *x* axis. The paths are recombined at beam splitter *N*, and the photon is observed by one of two detectors. The detour in the path of mode *b* is simply to ensure that the momentum kick is in the same direction for both mirrors.

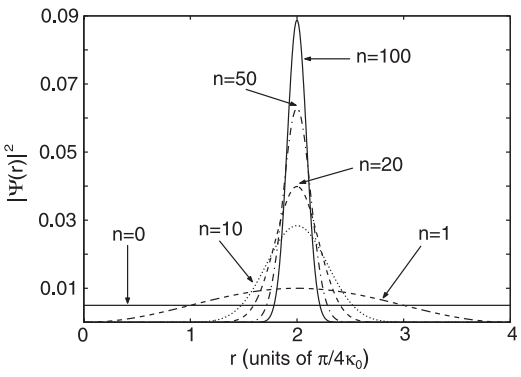

Fig. 2. Representative evolution of the mirror wave function for a monochromatic interferometer, over one period of localization. Each curve represents the relative-position probability distribution after *n* scattering events.

through without scattering. Therefore, the total state of the system just before detection, after removing the common phase, is

$$|\Psi_n\rangle = \sum_r c_r|r\rangle\left[\int_0^{2\pi}\frac{1}{2\sqrt{2\pi}}(e^{ik_\gamma r\sin\theta} + e^{-ik_\gamma r\sin\theta})|\theta\rangle d\theta + A(r)|0\rangle\right] \quad (8)$$

where the term proportional to $A(r) = \sqrt{\frac{1}{2\pi}\int_0^{2\pi}\sin^2(k_\gamma r\sin\theta')d\theta'}$ represents a nonscattering event that leaves the photon in $|0\rangle$ (*13*). The probability density (P_S) for detecting a scattered photon at $\theta \neq 0$ is given by

$$P_S(\theta) = \langle\Psi_n|\hat{a}_\theta^\dagger\hat{a}_\theta|\Psi_n\rangle = \frac{1}{2\pi}\sum_r|c_r|^2\cos^2(k_\gamma r\sin\theta) \quad (9)$$

where $\hat{a}_\theta$ is the annihilation operator of the corresponding mode $|\theta\rangle$. The probability of a nonscattering event is $P_{NS} = \Sigma_r|c_r|^2A^2 = 1 - \int_0^{2\pi}P_S(\theta)\,d\theta$, as required. If a scattered photon is detected at θ, the particles' wave function is accordingly updated

$$|\psi_{n+1}\rangle = \hat{a}_\theta|\Psi_n\rangle = \frac{1}{\sqrt{2\pi}}\sum_r c_r\cos(k_\gamma r\sin\theta)|r\rangle \quad (10)$$

Furthermore, a nonscattering event also changes their wave function: $|\psi_{n+1}\rangle = \Sigma_r c_r A(r)|r\rangle$. By renormalizing and iterating this procedure, we can simulate the localization of a pair of particles.

The particles are again taken to be in some initial state of ill-defined relative position over $r \in [0, L]$. It turns out that if all the photons are scattered, then the scattering process localizes the particles to $r = 0$. This can be understood from Eq. 10, as the cosine scattering envelope peaks at $r = 0$, irrespective of the observed angle of scattering, thus driving the particles toward zero separation. Physically, the two collocated particles act as a single point scatterer and the photon scatters isotropically. However, because the total scattering rate depends on r, a nonscattering event also yields information about the separation of the particles. In particular, a nonscattering event implies that the particles cannot have zero separation [because $A(0) = 0$]. In general, we observe both scattering and nonscattering events, and the particles localize to a different relative position for each sequence of detections, as was seen in the interferometer case. However, the wave function now becomes a single sharp peak in relative-position space even for photons of a single frequency, as the momentum kick varies with the angle of scattering.

As the particles localize in relative-position space, an interference pattern for the scattered photons emerges on the screen in the background. This can be understood in the context of a standard Young's-slit experiment, in which the visibility of the interference fringes depends on the degree of "which path" information available (*14*). Initially, the particles begin in delocalized states of well-defined momentum, so the momentum kicks imparted during the scattering process could in principle distinguish which particle recoiled (i.e., the two terms in the superposition of Eq. 1 are orthogonal). Thus, there is no interference for the first scattered photon. Nevertheless, our measurement process is not sensitive to this which-path information and entangles the two particles. As the localization process continues, however, their relative position becomes increasingly well defined. The resulting spread in their momentum distribution washes out the path distinguishability, and the familiar Young's interference pattern emerges (as follows from Eq. 9 when r is well defined). These characteristics of the localization process are consistent with experimental observations of interference from light scattering off a pair of trapped atoms (*15*).

Once the interference pattern of the scattered photons has stabilized, the feedback process ensures that subsequent scattering events only reinforce localization at existing separations. The localization is therefore robust to further measurements, meaning that relative position can be considered a classical property of the mirrors or particles, in the same sense that classicality is often defined in the decoherence literature [e.g., (*16*)].

The mathematical framework underlying the localization process can be derived entirely from the commutation relation of the position and momentum operators. Similar effects have also been established for the case of the number and phase operators, where a definite relative phase arises between two Bose-Einstein condensates due to number-space entanglement (*17*, *18*). This suggests that some form of entanglement-driven localization might occur for any pair of relative conjugate observables.

Finally, as discussed earlier, the wave function is in a center-of-mass momentum eigenstate throughout the localization process; the absolute positions of the mirrors and particles therefore remain undefined. Relative position thus cannot be defined by their independent existence at different locations on a coordinate system, as is the case for classical particles. Instead, it arises from the scattering-induced entanglement between the two particles. It can be shown that this entanglement is not disturbed when one of the pair is entangled with a third particle, and that the resulting relative positions are transitive: $r_{ab} + r_{bc} = r_{ac}$. Thus, we have a consistent definition of relative position that implies that relationships between objects, rather than coordinates and absolute variables, are fundamental in the quantum world.

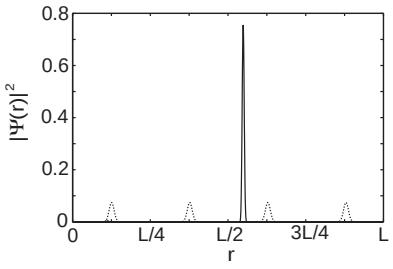

Fig. 3. Localization of the wave function after $n = 50$ scattering events with photons of variable frequency. A single peak exists in the entire region of size L. The dotted line is the $n = 100$ wave function from the monochromatic case of Fig. 2, which has multiple periods over the same region.

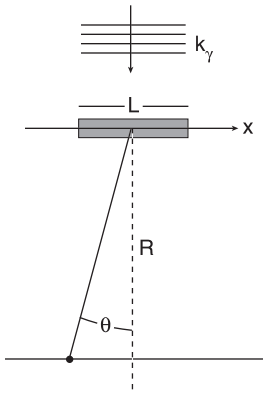

Fig. 4. General case of light scattering off a pair of particles that are initially delocalized in some region of size L. The incident photons are in plane wave states, and after scattering off the two particles are observed at some point on a screen at a distance R in the background ($R \gg L$).

References and Notes

1. E. Joos, H. D. Zeh, *Z. Phys. B* **59**, 223 (1985).
2. W. H. Zurek, *Phys. Today* **44**, 36 (1991).
3. G. C. Ghirardi, A. Rimini, T. Weber, *Phys. Rev. D* **34**, 470 (1986).
4. D. Giulini *et al.*, *Decoherence and the Appearance of a Classical World in Quantum Theory* (Springer, New York, 1996).
5. W. H. Zurek, *Rev. Mod. Phys.* **75**, 715 (2003).
6. C. Cabrillo, J. I. Cirac, P. Garcia-Fernandez, P. Zoller, *Phys. Rev. A* **59**, 1025 (1999).
7. Eq. 1 is a representation of the transition from initial to final states of the particles as a result of the entanglement with and subsequent detection of the photon. A more rigorous treatment is presented later in the paper.
8. V. Vedral, M. B. Plenio, M. A. Rippin, P. L. Knight, *Phys. Rev. Lett.* **78**, 2275 (1997).
9. M. Holland, S. Marksteiner, P. Marte, P. Zoller, *Phys. Rev. Lett.* **76**, 3683 (1996).
10. Introducing a lens requires a sum over all paths from particle to detector through the non-zero aperture of the lens, which gives a superposition of many momentum kicks to the particle [hence the integral in Eq. 4 of (*9*)], thus reducing its position uncertainty.

11. S. Barnett, P. Radmore, *Methods in Theoretical Quantum Optics* (Oxford Univ. Press, Oxford, 1997).
12. P. Hariharan, *Basics of Interferometry* (Academic Press, New York, 1992).
13. The nonscattering term depends on the total scattering rate over all angles (a function of *r*) and can be derived from the optical theorem (*19*). Additional considerations of scattering efficiency are straightforward and only affect the rate of localization.
14. S. M. Tan, D. F. Walls, *Phys. Rev. A* **47**, 4663 (1993).
15. U. Eichmann *et al.*, *Phys. Rev. Lett.* **70**, 2359 (1993).
16. M. Tegmark, J. A. Wheeler, *Sci. Am.* **284**, 68 (2001).
17. J. Javanainen, S. M. Yoo, *Phys. Rev. Lett.* **76**, 161 (1996).
18. J. A. Dunningham, K. Burnett, *Phys. Rev. Lett.* **82**, 3729 (1999).
19. L. Schiff, *Quantum Mechanics* (McGraw Hill, New York, 1968).

20. We thank A. R. P. Rau and W. D. Phillips for many helpful discussions. Supported by the National Science Foundation; the Marshall Aid Commemoration Commission; Merton College, Oxford; the UK Engineering and Physical Sciences Research Council; The Royal Society and Wolfson Foundation; and the European Union through the Cold Quantum Gases network.

24 March 2003; accepted 10 July 2003

Spectroscopic Identification of Carbonate Minerals in the Martian Dust

Joshua L. Bandfield,* Timothy D. Glotch, Philip R. Christensen

Thermal infrared spectra of the martian surface indicate the presence of small concentrations (~2 to 5 weight %) of carbonates, specifically dominated by magnesite ($MgCO_3$). The carbonates are widely distributed in the martian dust, and there is no indication of a concentrated source. The presence of small concentrations of carbonate minerals in the surface dust and in martian meteorites can sequester several bars of atmospheric carbon dioxide and may have been an important sink for a thicker carbon dioxide atmosphere in the martian past.

Carbonate minerals play an important role in determining the history of the martian atmosphere, geology, and hydrology. Specifically, carbonate minerals provide a trace for the presence of liquid water in the martian past and form readily in a CO_2 atmosphere when water is present (*1*, *2*). Carbonate minerals are also a potential sink of atmospheric CO_2 because there is no known widespread carbonate-recycling mechanism present on Mars such as plate tectonics on Earth. This sink may have important implications as regards the fate of a potentially thicker past martian atmosphere. Determining the quantity, form, and distribution of carbonate minerals on Mars is key to a basic understanding of the evolution of water and the atmosphere and to determining local climatic conditions in the martian past suitable for sustaining life.

Carbonate minerals have unique absorptions throughout the near-infrared and thermal infrared spectral regions (*3*–*6*) with overtone and combination bands at 2.35, 2.55, and 4.0 μm, and fundamental absorptions near 7, 11, and 30 μm. However, definitive identification of carbonate minerals on Mars has remained elusive (*7*–*10*).

Researchers used the Viking labeled release experiment to limit the concentration of carbonates present in the martian soil to levels near 1 to 2% in the presence of smectite clays (*11*, *12*). These low levels, as well as the lack of spectroscopic evidence for carbonates, have driven investigations of mechanisms such as ultraviolet photodissociation and acid-fog weathering (*13*, *14*) that may be responsible for the lack of carbonate minerals on Mars. Carbonate minerals have been found in low concentrations (up to ~1 weight %) in several martian meteorites (*15*), indicating that they must be present at some locations on Mars.

The systematic coverage, radiometric accuracy, and multiple emission angle observations of the Thermal Emission Spectrometer (TES) data have allowed for the isolation of the thermal infrared emissivity spectra of the surface dust (*16*) (Fig. 1). These data allow for characterization of the surface and atmospheric properties and separation of the surface and atmospheric contributions to the spectra (*16*). The multiple emission angle observation data use the aerosol opacity information retrieved from each observation to remove aerosol effects and produce quantitative surface emissivities (*17*).

We selected 21 multiple emission angle sequences from a variety of dust-covered, high-albedo regions between 30°S and 15°N, and the surface emissivity was retrieved (*17*) (Fig. 1). All surface spectra have the same spectral character, including a relatively narrow absorption near 830 cm^{-1} and a broad, deep absorption at >1250 cm^{-1}. A superimposed, narrower emissivity minimum is located near 1580 cm^{-1} with a local emissivity maximum near 1630 cm^{-1}. A prominent convex spectral curve is present from 1450 to 1580 cm^{-1}. There is little to no absorption at frequencies <550 cm^{-1} and between 900 and 1250 cm^{-1}. The standard deviation in the spectral shape of the surfaces is <0.01 from 250 to 1610 cm^{-1} and climbs from 0.01 to 0.02 from 1620 to 1650 cm^{-1} (Fig. 1).

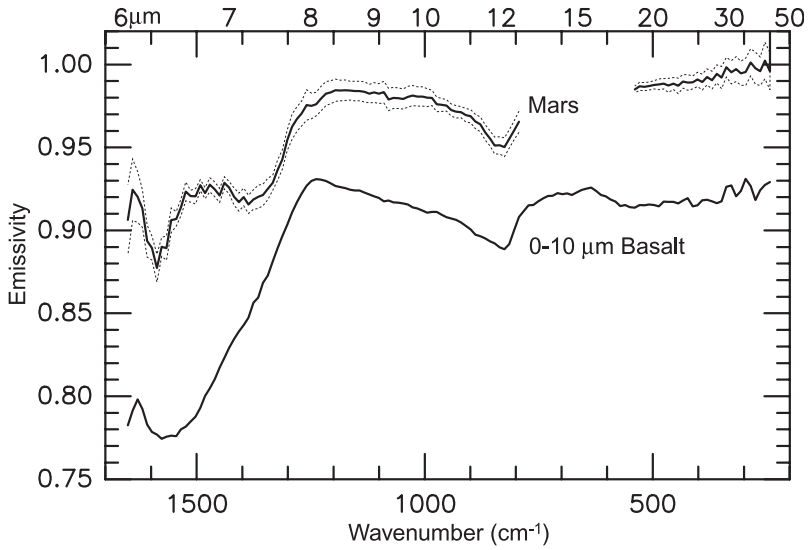

Fig. 1. Mars high-albedo surface dust spectrum (top, solid line) ± SD (dashed lines). A fine-particulate basalt spectrum (solid line, offset) displays similar spectral features from 200 to 1300 cm^{-1} due to its high plagioclase content. Similar to other silicates, sulfates, and oxides, the spectrum does not match well at >1300 cm^{-1}. Bound or adsorbed water is present in the basalt sample, resulting in the emission peak near 1620 cm^{-1}.

Department of Geological Sciences, Arizona State University, Tempe, AZ 85287–6305, USA.

*To whom correspondence should be addressed. E-mail: joshband@asu.edu